Electronic Supplementary Material (ESI) for Materials Horizons.
This journal is © The Royal Society of Chemistry 2024

Supplementary Information

Floquet engineering of orbital Hall effect and valleytronics in two-dimensional topological magnets

Runhan Li,[1] Xiaorong Zou,[1] Zhiqi Chen,[1] Xiaoran Feng,[1] Baibiao Huang,[1] Ying Dai,[1], * and Chengwang Niu[1], *

[1]School of Physics, State Key Laboratory of Crystal Materials, Shandong University, Jinan 250100, China

S1 Computational method

First-principles calculations were conducted within the framework of density functional theory (DFT) employing the projector augmented wave (PAW) method as implemented in the Vienna ab initio simulation package (VASP) [1, 2]. The Perdew-Burke-Ernzerhof (PBE) formulation of the generalized gradient approximation (GGA) was employed for the exchange-correlation potential [3]. A cutoff energy of 500 eV was utilized, and structural relaxation was performed until the residual forces were below 0.01 eV/Å. To account for the Coulomb interaction, the GGA+U method with a U value of 3 eV for the Sc-*d* electrons was employed. To identify its topology, we construct triangular nanoflakes of ScI_2 monolayer with 87 Å on each edge, which ensures that the nanoflakes have a large enough width to avoid the interactions among different corners. The construction of maximally localized Wannier functions (MLWFs) was constructed in the basis of Sc-*d* and I-*p* orbitals using the WANNIER90 code [4], which combined the results of first-principles calculations from VASP. The surface density of states is obtained by the iterative Green's function method [5].

S2 Floquet Effective $k \cdot p$ Hamiltonian with out-of -plane magnetic field

Assuming $m > \Delta > \lambda$ and focusing solely on the two lowest energy bands. With out-of-plane magnetic field, the energy can be obtained through matrix diagonalization:

$$E_{c/v}(\tau) = \frac{1}{2}[2e - \tau\lambda - 2m \pm \sqrt{(\Delta + \tau\lambda)^2 + 4t^2(k_x^2 + k_y^2)}].$$

At $\mathbf{q} = 0$, the energy of valleys is $E_c(\tau,\eta) = e + \frac{\Delta}{2} - m$, and $E_v(\tau,\eta) = e - \frac{\Delta}{2} - m - \tau\lambda$. Based on Floquet theory, when a CPL is applied, the $k \cdot p$ Hamiltonian can be periodic in time $H(t) = H(t+T)$. By Peierls substitution $\mathbf{k} \to \mathbf{k} + e\mathbf{A}/\hbar$, time-dependent Hamiltonian is obtained. $\mathbf{A} = A[\cos(\omega t)\mathbf{e}_1 + \eta \sin(\omega t)\mathbf{e}_2]$ is the vector potential of the CPL, where $\eta = \pm 1$ denotes the left/right-handed CPL, A and ω is the amplitude and frequency of vector potential.

Considering the Floquet theory in the high-frequency (ω) limit, the effective time-independent Hamiltonian describing the light driven system can be formulated as

$$H_{\text{eff}}(\mathbf{k}) = H_0(\mathbf{k}) + \sum_{n\geqslant 1} \frac{[H_{-n}, H_n]}{n\omega} + O\left(\frac{1}{\omega^2}\right),$$

where $H_{\pm n} = \frac{1}{T}\int_0^T d\tau e^{\pm in\omega t} H(t)$ is the Fourier component in the frequency space and $T = 2\pi/\omega$ is the period of the CPL. By explicitly calculating high-frequency expansion up to first-order term, we have the effective Hamiltonian

$$H_{\text{eff}}(\mathbf{k}) = H(\mathbf{k}) + I_2 \otimes (d_1 - d_2)\sigma_z,$$

where $d_1 = \frac{\tau A(\eta k_x + 2\pi k_y)}{\omega^3}$ and $d_2 = \frac{\tau\eta A^2\left(4\pi^2 - 1\right)}{4\omega^3}$. The energy of two valleys under CPL with out-of-plane magnetic field can be obtained:

$$E_c(\tau,\eta) = e + \frac{\Delta}{2} - m - \frac{\tau\eta A^2\left(4\pi^2 - 1\right)}{4\omega^3},$$

$$E_v(\tau,\eta) = e - \frac{\Delta}{2} - m - \tau\lambda + \frac{\tau\eta A^2\left(4\pi^2 - 1\right)}{4\omega^3}.$$

To simplify the analysis of light's effect on valleys, we initially assume $\lambda = 0$ for the SOC effect. Subsequently, we can get the energy gap $E_g(\tau,\eta) = \Delta - \frac{\tau\eta A^2\left(4\pi^2 - 1\right)}{2\omega^3}$ at the two valleys. Appling the left-handed CPL, the energy difference between the band gap at K' valley and K valley is $\frac{A^2\left(4\pi^2 - 1\right)}{\omega^3}$. This result implies that, under the influence of CPL, valley degeneracy is broken, leading to simultaneous valley polarization in both the valence and conduction bands. The magnitude of valley polarization depends on the amplitude of light. With increasing amplitude of light, valley splitting enlarges, and the gap decreases. It is noteworthy that when $\Delta = \frac{\tau\eta A^2\left(4\pi^2 - 1\right)}{2\omega^3}$, the K valley closes and leading the system to a half-valley metal state. Under the application of right-handed CPL, increasing amplitude of light leads to gap closure in the opposite valley. In the presence of a nonzero λ, spontaneous valley polarization emerges, but with increasing light intensity, it will still become a half-valley metal state. Upon further examination of the second-order term, $\frac{[H_{-2}, H_2]}{n\omega} = I_2 \otimes \frac{-2\tau\eta A(3k_x + 4A)}{9\omega^3}\sigma_z$, it can be found that the effect of the higher order term is similar to that of the first order term, where the correction to the valley energy is likewise influenced by the magnitude of amplitude of light.

S3 Detailed analysis for the Floquet tight-binding Hamiltonian

Here, a symmetry constrained tight-binding (TB) model has been constructed based on the $d_{z^2,\uparrow}, d_{xy,\uparrow}, d_{x^2-y^2,\uparrow}, d_{z^2,\downarrow}, d_{xy,\downarrow}, d_{x^2-y^2,\downarrow}$ orbitals with spin. This TB model for the magnetic monolayer can be expressed as follows:

$$H = \sum_{\langle i,j \rangle} \sum_{m,n} t_{j-i}^{mn} c_m^{\dagger}(\mathbf{r}_i) c_n(\mathbf{r}_j),$$

where $c_n^{\dagger}(\mathbf{r}_i)$ ($c_{n'}(\mathbf{r}_j)$) represents the creation (annihilation) operator for an electron on site i (site j), where m, n denotes different orbitals with spin. Given the constraint of D_{3h} point group symmetry, the intra-layer hopping terms are reduced to six parameters, while the inter-layer hopping terms are simplified to two parameters.

Under the constraint of D_{3h} point group symmetry, the intra-layer hopping terms are reduced to eight parameters, while the inter-layer hopping terms are reduced to two parameters while preserving spin degeneracy. The Hamiltonian $H_0(k)$ in the momentum space representation under the constraint of symmetry operation *R* can be written as

$$P(R)^{-1} H(\boldsymbol{k}) P(R) = H(\hat{R}^{-1}\boldsymbol{k}).$$

The point group D_{3h} contains discrete rotation symmetry C_3 (the axis is perpendicular to the plane), mirror symmetry M_z, mirror symmetry M_x, and any of their combination. Considering symmetry restrictions on the model hopping parameters, we start from the three-band nearest-neighbor hopping TB model for the TMDs monolayer, and the Hamiltonian can be expressed as [6]

$$H_0(\mathbf{k}) = \begin{bmatrix} h_{11} & h_{12} & h_{13} & & & \\ h_{12}^* & h_{22} & h_{23} & & & \\ h_{13}^* & h_{23}^* & h_{33} & & & \\ & & & h_{11} & h_{12} & h_{13} \\ & & & h_{12}^* & h_{22} & h_{23} \\ & & & h_{13}^* & h_{23}^* & h_{33} \end{bmatrix},$$

where

$$h_{11} = 2t_1(\cos 2\alpha + 2\cos\alpha\cos\beta) + \epsilon_1,$$

$$h_{12} = -2\sqrt{3}t_3 \sin\alpha \sin\beta + 2it_2(\sin 2\alpha + \sin\alpha\cos\beta),$$

$$h_{13} = 2t_3(\cos 2\alpha - \cos\alpha\cos\beta) + 2\sqrt{3}it_2 \cos\alpha\sin\beta,$$

$$h_{22} = 2t_4 \cos 2\alpha + (t_4 + 3t_6)\cos\alpha\cos\beta + \epsilon_2,$$

$$h_{23} = \sqrt{3}(t_6 - t_4)\sin\alpha\sin\beta + 4it_5 \sin\alpha(\cos\alpha - \cos\beta),$$

$$h_{33} = 2t_6 \cos 2\alpha + (3t_4 + t_6)\cos\alpha\cos\beta + \epsilon_2,$$

$$(\alpha, \beta) = (\frac{1}{2}k_x a, \frac{\sqrt{3}}{2}k_y a).$$

Subsequently, we further consider the interaction of spin-orbit coupling (SOC) by the on-site contribution term $\boldsymbol{L}\cdot\boldsymbol{S}$ and magnetic field interactions, and add the two terms to the model as:

$$H(\boldsymbol{k}) = H_0(\boldsymbol{k}) + H_{SOC} + H_M .$$

In which

$$H_{SOC} = t_{so}\boldsymbol{L}\cdot\boldsymbol{S},$$

$$H_M = t_m\boldsymbol{B}\cdot\boldsymbol{S},$$

where H_{SOC} and H_M are on-site SOC interaction with strength t_{so} and exchange field (magnetic field) terms with strength t_m, respectively. $\mathbf{B} = (B_x, B_y, B_z)$ represents the directions of the magnetic field. t_{so} =0.2 eV and t_m =3.0 eV are used. With in-plane magnetic field, the conduction and valence bands around the Fermi level for the TB model have the same spin channel and possess a significant band gap.

When a time-periodic light field is applied to the TB model, the time dependent TB Hamiltonian can be written as

$$H(\mathbf{k}, t) = \sum_{m,n,j} t_j^{mn}(t) e^{i\mathbf{k}\cdot\mathbf{R}_j} c_m^+(\mathbf{k}, t) c_n(\mathbf{k}, t),$$

where the vector potential is coupled to the Hamiltonian through the minimal coupling of $t_j^{mn}(\tau) = t_j^{mn} e^{i\frac{e}{\hbar}\mathbf{A}(\tau)\cdot\mathbf{d}_j^{mn}}$, $\mathbf{d}_j^{mn}$ is the position vector between orbital *m* in 0 cell and orbital *n* in *j*-cell. Based on Floquet–Bloch theory, the effective static Hamiltonian can be written as [7]

$$H_F(\mathbf{k}, \omega) = \sum_{m,n,\alpha,\beta} \left[h_{\alpha-\beta}^{mn}(\mathbf{k}) + \alpha\hbar\omega\delta_{mn}\delta_{\alpha\beta} \right] c_{\alpha m}^+(\mathbf{k}) c_{\beta n}(\mathbf{k}),$$

$$h_q^{mn}(\mathbf{k}) = \sum_j t_j^{mn} \cdot J_q \left[\frac{e}{\hbar}\mathbf{A}(\tau)\cdot\mathbf{d}_j^{mn} \right] \cdot e^{i\mathbf{k}\cdot\mathbf{R}_j},$$

$$J_q \left[\frac{e}{\hbar}\mathbf{A}(\tau)\cdot\mathbf{d}_j^{mn} \right] = \frac{1}{T}\int_0^T e^{i\left[\frac{e}{\hbar}\mathbf{A}(\tau)\cdot\mathbf{d}_j^{mn} + q\omega t\right]} d\tau,$$

where $h_{\alpha-\beta}^{mn}(\mathbf{k})$ is the matrix element of the q th part of the Floquet matrix, and J_q is the q-th Bessel function of the first kind. Because larger values of q, J_q decrease more rapidly to zero with weak light intensity, it is only necessary to include a few lowest-order photon processes into

H_F, and this can restrict it to a finite dimension. Here, desirable convergence results can be reached by considering only the first-order term of J_q. In our work, $\hbar\omega = 12\text{eV}$ is chosen to be larger than bandwidth so that the Floquet bands do not cross each other. A comparison of the band structures considering both the first-order and second-order truncated terms with different light intensities is shown in the figure below.

Table S1. The parameters amplitudes in eV of the TB model with SOC and exchange field terms.

hopping	ϵ_1	ϵ_2	t_1	t_2	t_3
	t_4	t_5	t_6	t_{so}	t_m
strength	1.746	2.804	−0.184	0.401	0.507
	0.218	0.338	0.057	0.2	3.0

S4 Orbital Hall conductivity and orbital weighted Berry curvature

We can calculate the orbital Hall conductivity (OHC) responses to an applied electric field. Up to linear order on the external field, they are given by

$$\sigma_{xy}^{o} = \frac{e}{(2\pi)^2}\sum_n \int_{\text{BZ}} d^2k f_{n\mathbf{k}} \Omega_{n,ij}^{O,z},$$

where σ_{xy}^{o} is the OHC with polarization along the z direction, and

$$\Omega_{n,ij}^{O,z}(\mathbf{k}) = 2\hbar\text{Im}\sum_{m\neq n} \frac{\left\langle u_{\mathbf{k}}^n \middle| \mathcal{J}_{o,i}^z \middle| u_{\mathbf{k}}^m \right\rangle \left\langle u_{\mathbf{k}}^m \middle| \hat{v}_j \middle| u_{\mathbf{k}}^n \right\rangle}{(\varepsilon_{\mathbf{k}}^n - \varepsilon_{\mathbf{k}}^m)^2},$$

represents the Berry curvature weighted by angular momentum. Here, $\varepsilon_{\mathbf{k}}^n$ represents the eigenvalue of the Hamiltonian $H(\vec{k})$ in reciprocal space, and $u_{\mathbf{k}}^m$ corresponds to the eigenvector. In this context, n signifies the band index, and $\vec{k}$ denotes the wave vector. The velocity operator denotes as $\hat{v}_{x(y)}(\vec{k}) = \partial H(\vec{k}) / \partial \hbar k_{x(y)}$, with x and y specifying the Cartesian axes, and we assume that the electric field is applied along the $\hat{x}$ direction. The orbital angular momentum current density operator is defined as $\mathcal{J}_{o,i}^z = \left[\ell_z v_y(\vec{k}) + v_y(\vec{k})\ell_z\right]/2$, where ℓ_η represent the z components of the atomic angular momentum operators.

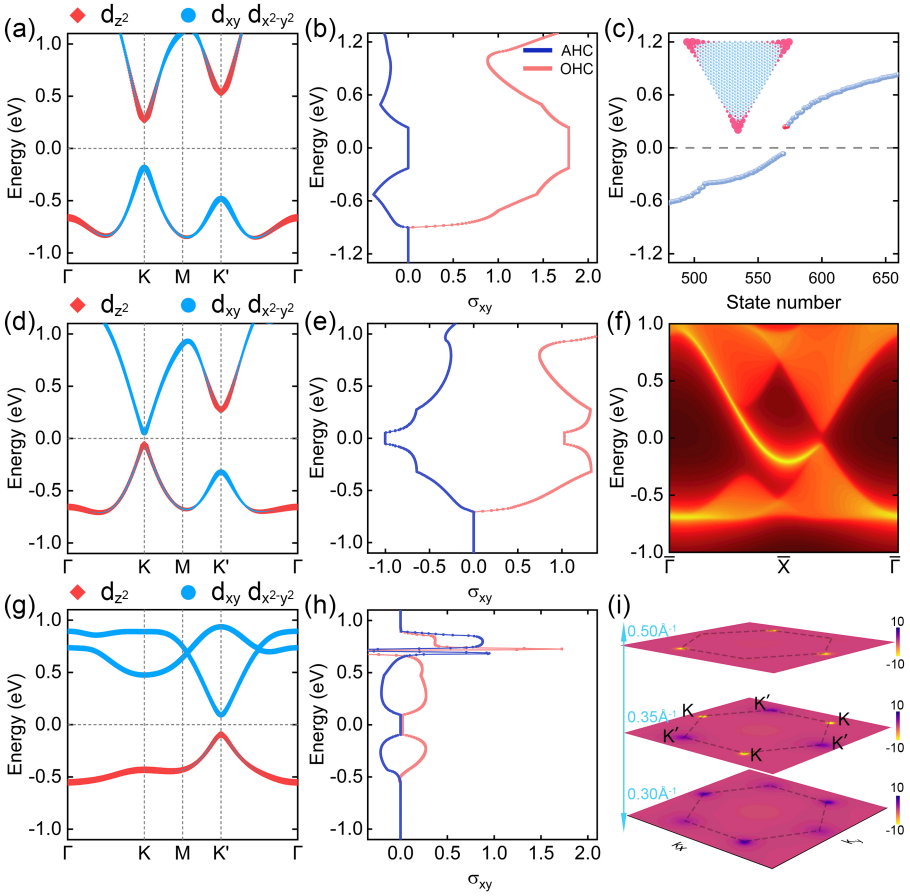

Figure S1 Orbital-resolved band structures and energy dependence of the anomalous Hall conductivity (AHC) and orbital Hall conductivity (OHC) for the TB model with in-plane magnetization under the irradiation of right-handed CPL with light intensity $eA/\hbar$ of (a, b) 0.7 Å^{-1}, (d, e) 0.9 Å^{-1}, and (g, h) 1.2 Å^{-1}, respectively. Red and blue lines in (b, e, h) represent the OHC (unit $e/2\pi$) and AHC (unit e^2/h), respectively. (c) Energy spectrum of the triangle-shaped nanoflake for the TB model with light intensity $eA/\hbar$ of 0.7 Å^{-1}, where red dots mark the nontrivial corner states. Inset presents the total charge distribution of the nontrivial corner states. (f) Energy dispersion of a semi-infinite nanoribbon for the TB model with a light intensity $eA/\hbar$ of 0.9 Å^{-1}, revealing characteristic chiral edge states due to the nontrivial QAHE. (i) *K*-space distributions of orbital Berry curvature under right-handed CPL with multiple topological states.

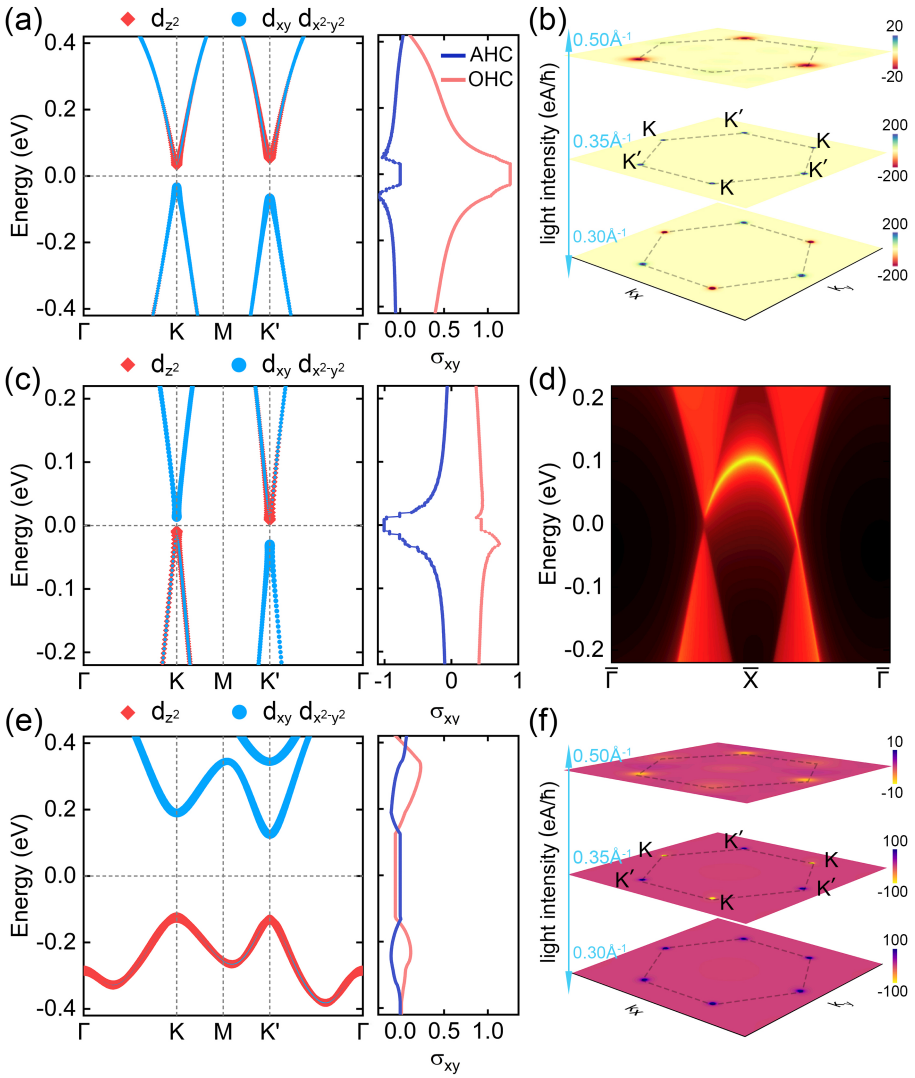

Figure S2 Orbital-resolved band structures and energy dependence of AHC and OHC for ScI_2 monolayer with in-plane ferromagnetism under the irradiation of right-handed CPL with light intensity $eA/\hbar$ of (a) 0.30 Å^{-1}, (c) 0.35 Å^{-1}, and (e) 0.50 Å^{-1}, respectively. *K*-space distributions of (b) Berry curvature and (f) orbital Berry curvature under right-handed CPL with multiple topological states. (d) Energy dispersion of a semi-infinite nanoribbon for ScI_2 monolayer with a light intensity $eA/\hbar$ of 0.35 Å^{-1}, revealing characteristic chiral edge states due to the nontrivial QAHE.

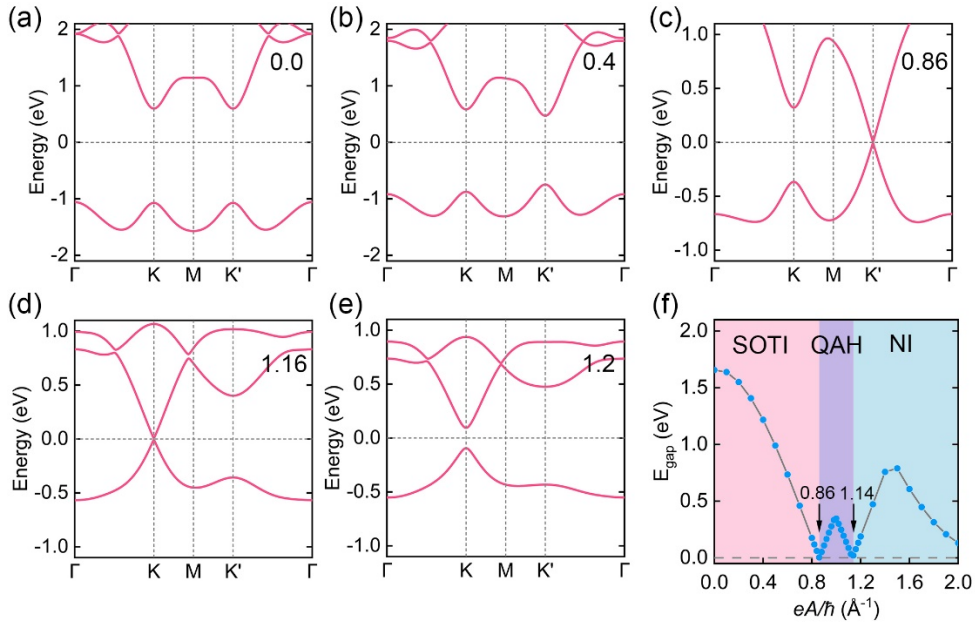

Figure S3 Band structure of the TB model with an in-plane magnetic field under the irradiation of left-handed CPL with light intensity $eA/\hbar$ of (a) 0.0 Å^{-1}, (b) 0.4 Å^{-1}, (c) 0.86 Å^{-1}, (d) 1.16 Å^{-1}, (e) 1.2 Å^{-1}, respectively. (f) Phase diagram of the TB model with an in-plane magnetic field as a function of light intensity. CPL can drive multiple phase transitions from a second-order topological insulator (SOTI) to a valley-polarized Quantum Anomalous Hall (QAH) phase and subsequently to a normal insulator (NI) state.

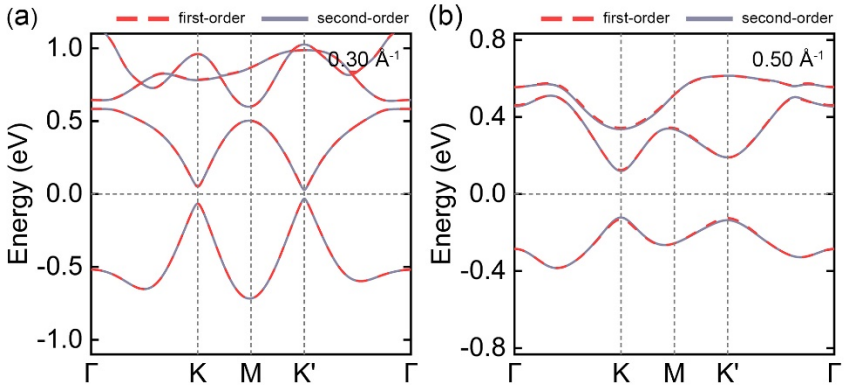

Figure S4 The Floquet band structures of ScI_2 monolayer among different truncated orders (q=1, 2) with light intensity $eA/\hbar$ of (a) 0.30 Å^{-1} and (b) 0.50 Å^{-1}, where dashed lines represent the first-order terms, and solid lines represent the second-order terms.

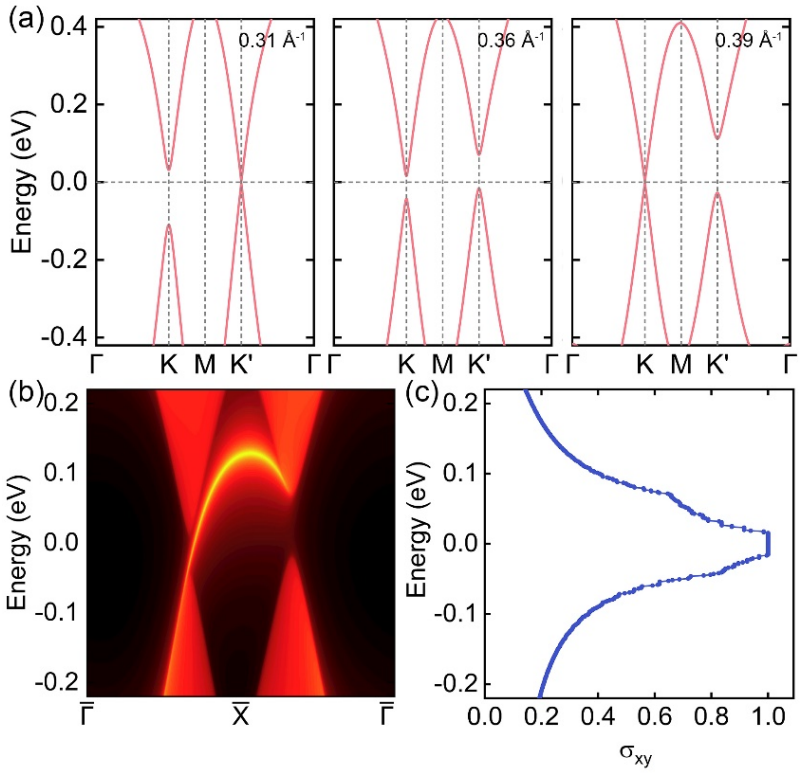

Figure S5 (a) The band structures for ScI_2 monolayer with out-of-plane ferromagnetism under the irradiation of left-handed CPL with light intensity $eA/\hbar$ of 0.31 Å^{-1}, 0.36 Å^{-1}, and 0.39 Å^{-1}, respectively. (b) Energy dispersion of a semi-infinite nanoribbon for ScI_2 monolayer with a light intensity $eA/\hbar$ of 0.36 Å^{-1}. (c) Energy dependence of anomalous Hall conductivity with light intensity $eA/\hbar$ of 0.36 Å^{-1}. Under light irradiation, band closures occur successively at the K' and K points, indicating that the system with out-of-plane ferromagnetism can undergo two topological phase transitions.

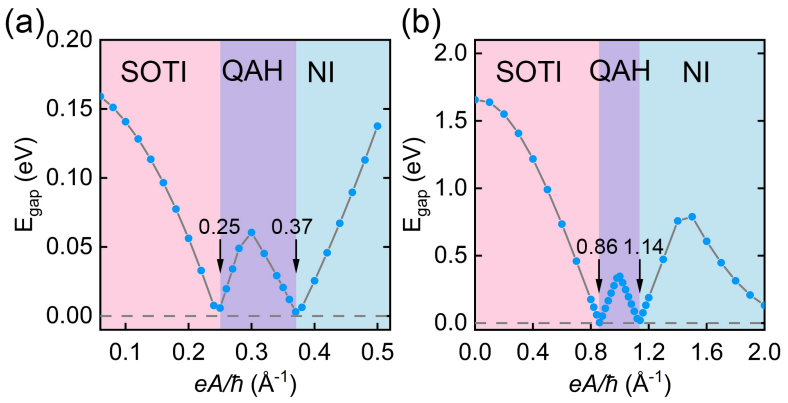

Figure S6 Phase diagrams of the TB model with an in-plane magnetic field as a function of light intensity for (a) ϵ_2-ϵ_1 = 2.558 (smaller band gap) and (b) ϵ_2-ϵ_1= 1.058 (larger band gap), respectively. In both cases, CPL can drive multiple phase transitions from a SOTI to a QAH phase and subsequently to a NI state.

References

[1] G. Kresse and J. Hafner, Phys. Rev. B 47, 558 (1993).

[2] G. Kresse and J. Furthmüller, Phys. Rev. B 54, 11169 (1996).

[3] J. P. Perdew, K. Burke, and M. Ernzerhof, Phys. Rev. Lett. 77, 3865 (1996).

[4] A. A. Mostofi, J. R. Yates, Y.-S. Lee, I. Souza, D. Vanderbilt, and N. Marzari, Comput. Phys. Commun. 178, 685 (2008).

[5] Q. Wu, S. Zhang, H.-F. Song, M. Troyer and A. A. Soluyanov, Comput. Phys. Commun., 224, 405 (2018).

[6] Liu, G.-B.; Shan, W.-Y.; Yao, Y.; Yao, W.; Xiao, D. Phys. Rev. B 88, 085433 (2013).

[7] Z. F. Wang, Z. Liu, J. Yang and F. Liu, Phys. Rev. Lett., 120, 156406 (2018)